RSC Advances

PAPER

View Article Online
View Journal | View Issue

Check for updates

Cite this: *RSC Adv.*, 2020, **10**, 33499

Hydrothermal control, characterization, growth mechanism, and photoluminescence properties of highly crystalline 1D $Eu(OH)_3$ nanostructures†

Xiang Ji,‡[a] Pingjing Hu,‡[a] Xiangzi Li,*[ab] Longwei Zhang‡[a] and Jian Sun[b]

Received 15th May 2020
Accepted 3rd September 2020

DOI: 10.1039/d0ra04338a

rsc.li/rsc-advances

Six types of 1D $Eu(OH)_3$ nanostructures with typical morphologies, including short hexagonal prism, long hexagonal prism, coiling rod, short rod, long rod, and nanobunch, were synthesized *via* the hydrothermal route using $EuCl_3$ and NaOH as raw materials. The morphologies, sizes, structures, and compositions of the as-prepared products were characterized by scanning electron microscopy, transmission electron microscopy, selected area electron diffraction, X-ray diffraction, and Fourier transform infrared spectroscopy. The effects of different reaction conditions on the morphology and size of the products were also investigated, and the relevant growth mechanism was assessed. Results showed that the geometric features of $Eu(OH)_3$ are affected by the precursor pH and reaction time and temperature; among these factors, precursor pH played a key role in controlling the morphologies of the resulting $Eu(OH)_3$ nanostructures. The fluorescence properties of the six $Eu(OH)_3$ nanostructures were analyzed, and typical photoluminescence emission peaks due to the $^5D_0$–^7F_J (J = 1–4) transition of Eu^{3+} were noted. Moreover, the intensity of the emission peak of the products at 616 nm was slightly weaker than that at 592 nm. This finding reflects the high site symmetry of Eu^{3+} in the $Eu(OH)_3$ nanostructures.

Open Access Article. Published on 10 September 2020. Downloaded on 6/2/2026 2:16:28 AM.
This article is licensed under a Creative Commons Attribution-NonCommercial 3.0 Unported Licence.

Introduction

Nanomaterials present excellent optical, electronic, magnetic, and mechanical properties on account of their unique small-size, surface, and quantum effects; as such, these materials have been widely applied to the field of catalysis, energy, environment, biomedicine, and aerospace, among others. The physical and chemical properties of nanomaterials mainly depend on their size, crystal form, and morphology; thus, materials bearing differences in these characteristics may show different properties even if they have the same chemical composition. The controlled synthesis of nanomaterials with different structures and geometric characteristics is an important challenge in efforts to obtain improved performance[1,2] from nanowires, nanorods, nanotubes, and nanobelts. Indeed, the synthesis of 1D nanomaterials is of particular interest because they may provide a foundation for the subsequent construction of nano-functional devices because of their quantum confinement effect.[3–5]

$Eu(OH)_3$ nanomaterials have good electronic, optical, and chemical properties arising from electron transitions within the 4f shell; thus, these materials maybe used in fluorescent,[6] magnetic,[7] and biological[8,9] applications. However, the structure of an $Eu(OH)_3$ nanomaterial can affect the binding state of Eu^{3+} or Eu in its micro-environment and, in turn, modulate the material's performance. Thus, controlling the size and shape of $Eu(OH)_3$ nanomaterials by using different methods is necessary. $Eu(OH)_3$ nanomaterial synthesis has become a research hotspot among scholars. Various $Eu(OH)_3$ nanostructures have also received a great amount of attention. However, to the best of our knowledge, there are few reports on the synthesis of diverse 1D $Eu(OH)_3$ nanostructures, except that Zhang *et al.* fabricated $Eu(OH)_3$ nanospindles, nanorods, and nanobundles by using $Eu(NO_3)_3$ and NaOH as starting reagents at room temperature for 12 h, and then investigated the influences of the molar ratio of $[OH^-]/[Eu^{3+}]$, reaction time and temperature on the reaction.[10] Up to now, precipitation or hydrothermal process have been widely employed to synthesize 1D $Eu(OH)_3$ nanostructures. For example, hexagonal-phase single-crystal $Eu(OH)_3$ (ref. 11) and D-glucuronic acid-coated $Eu(OH)_3$ (ref. 12) nanorods were individually obtained by a precipitation method using cyclohexylamine or NaOH pellets as alkaline source, in which the synthesis methods were relatively simple but provide relatively few adjustable factors to enable the complete control the structures of the resulting $Eu(NO_3)_3$ nanomaterials. As far as hydrothermal method is concerned, it presents numerous adjustable parameters and, hence, is widely

[a]*Anhui Province Key Laboratory of Active Biological Macro-molecules Research, Institute of Synthesis and Application of Medical Materials, Department of Chemistry, Wannan Medical College, Wuhu 241002, China. E-mail: li-xiang-zi@163.com*

[b]*College of Chemistry and Materials Science, Anhui Laboratory of Molecule-based Materials, Anhui Normal University, Wuhu 241002, China*

† Electronic supplementary information (ESI) available. See DOI: 10.1039/d0ra04338a

‡ Equal contribution as the first author.

Open Access Article. Published on 10 September 2020. Downloaded on 6/2/2026 2:16:28 AM.
This article is licensed under a Creative Commons Attribution-NonCommercial 3.0 Unported Licence.

used to prepare 1D rare-earth hydroxide nanostructures. For instance, in the presence of $Eu(NO_3)_3$ or Eu_2O_3, different scale 1D rod-like $Eu(OH)_3$ have also been obtained by a hydrothermal method using NaOH,[13,14] NH_3 (ref. 15) or KOH[16] as alkali. Despite the success of the above methods, however, $Eu(OH)_3$ nanostructures fabricated by hydrothermal technology usually have a large size, poor uniformity or single morphology; especially, reports on the precise structural control of 1D $Eu(OH)_3$ nanostructures fabricated through hydrothermal synthesis are scarce. We previously discussed several factors influencing the synthesis of metal nanotubes[17] and Ag_3PO_4 nanorods[18] during template deposition, similarly, it is also very significant to control precisely the structures of 1D $Eu(OH)_3$ nanostructures with hydrothermal technique.

In the present study, we report a controllable method to synthesize highly uniform single-crystalline 1D $Eu(OH)_3$ nanostructures using simple chemical reagents *via* the hydrothermal method, and explore the influences of pH, reaction time and temperature on the resulting microstructures in detail. The results of this study provide deeper insights into the structural regulation of $Eu(OH)_3$, which is also meaningful and could be referenced for the fabrication other nanostructures by hydrothermal technique.

Experimental section

Preparation of 1D $Eu(OH)_3$ nanostructures

Analytical-grade $EuCl_3 \cdot 6H_2O$, NaOH, and absolute alcohol were purchased from Sinopharm Chemical Regent Company (China) and used without further purification. Deionized water was used throughout the process. A typical synthesis procedure was conducted as follows. 39.5 mL of $EuCl_3$ aqueous solution (1.69 mmol L^{-1}) was stirred with a magnetic stirrer and then added drop-wise with 1.0 mmol L^{-1} NaOH aqueous solution followed by the adding of some water with total volume of 40 mL. The pH (8.88–12.50) of the solution was monitored using an acidity meter to obtain white precursor precipitates. The resulting mixture was then transferred to a 40 mL Teflon-lined stainless-steel autoclave, maintained at various temperatures (120–180 °C) for 20–35 h in an oven, and then cooled to room temperature. The resulting white precipitates were collected by

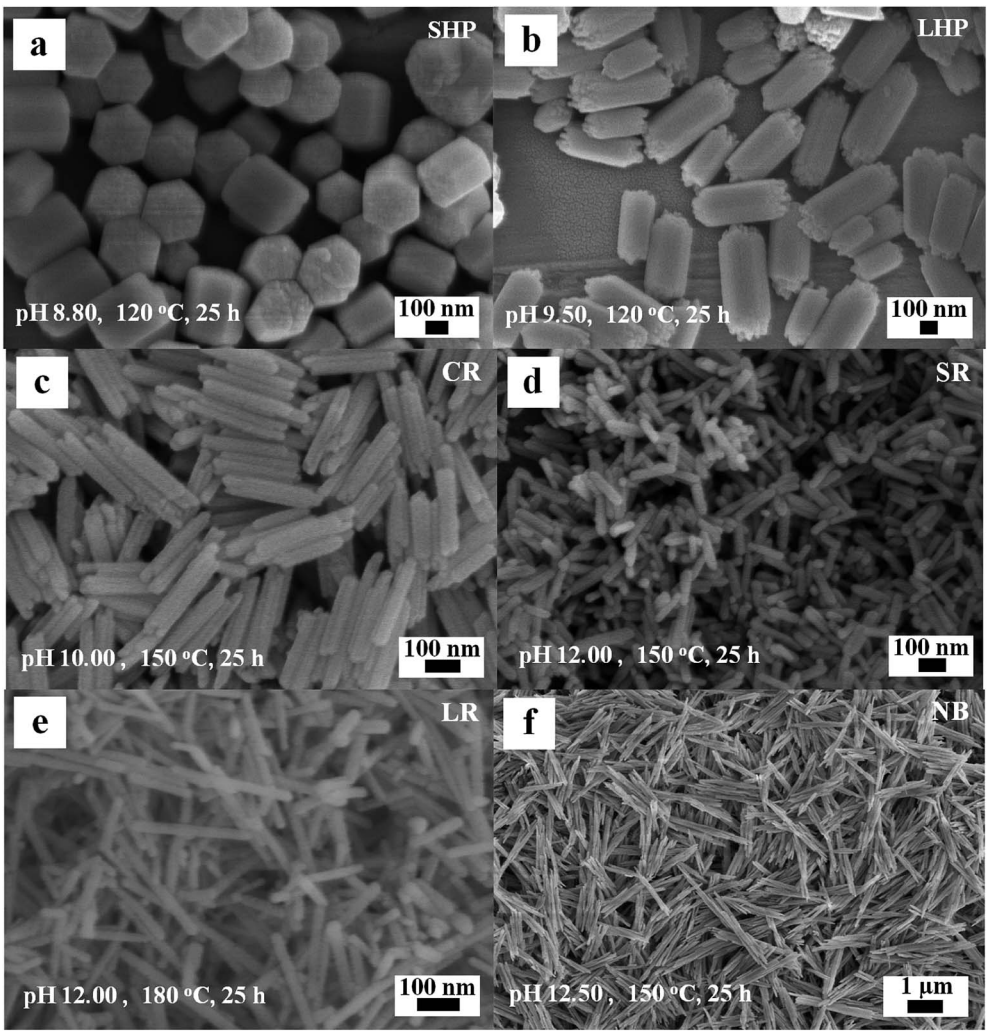

Fig. 1 SEM images of the typical $Eu(OH)_3$ nanostructures. (a) SHP. (b) LHP. (c) CR. (d) SR. (e) LR. (f) NB.

 This journal is © The Royal Society of Chemistry 2020

Open Access Article. Published on 10 September 2020. Downloaded on 6/2/2026 2:16:28 AM.
This article is licensed under a Creative Commons Attribution-NonCommercial 3.0 Unported Licence.

Table 1 The synthesis conditions and average sizes of the $Eu(OH)_3$ nanostructures

Shape	t (h)	pH	$\bar{T}$ (°C)	$\bar{L}$ (nm)	$\bar{D}$ (nm)	$\bar{L}/\bar{D}$
SHP	25	8.80	120	276 ± 15	246 ± 21	1.1
LHP	25	9.50	120	460 ± 62	219 ± 25	2.1
CR	25	10.00	150	258 ± 13	48 ± 5	5.3
SR	25	12.00	150	113 ± 21	29 ± 1	3.9
LR	25	12.00	180	274 ± 82	23 ± 3	11.8
NB	20	12.50	150	1719 ± 422	182 ± 48	9.4

centrifugation, washed repeatedly with deionized water and ethanol, and then dried in a vacuum.

Characterization

The surface morphologies of the as-prepared products were examined by a scanning electron microscope (SEM, Hitachi S-4800), and internal structures and crystalline phases were measured using a high-resolution transmission electron microscope (HRTEM, JEM-2010). The X-ray diffraction (XRD, MiniFlex-600) patterns of the as-prepared samples were recorded on a D/teX Ultra2 diffractometer, and Fourier transform

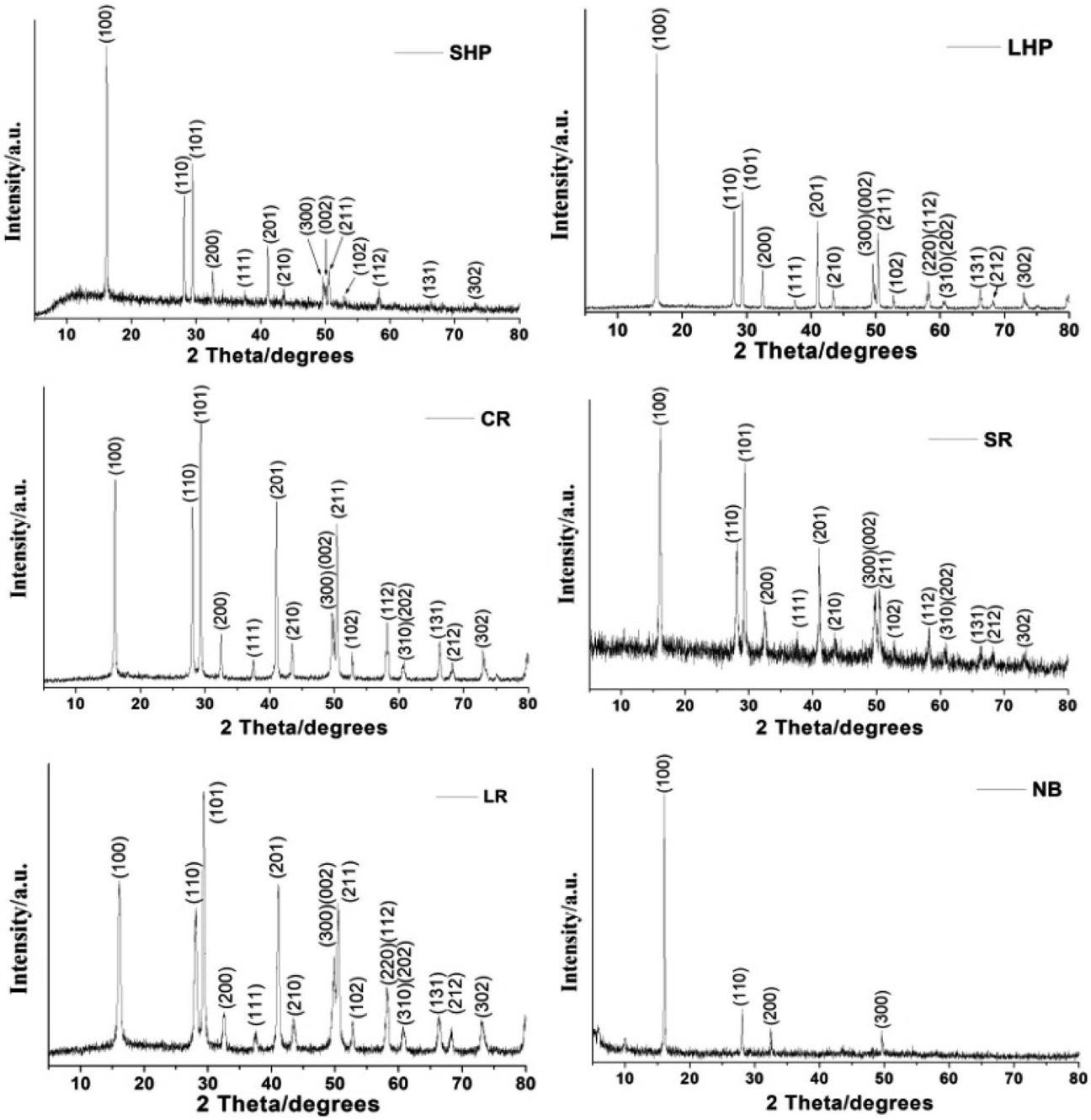

Fig. 2 XRD patterns of the typical $Eu(OH)_3$ nanostructures.

Open Access Article. Published on 10 September 2020. Downloaded on 6/2/2026 2:16:28 AM.
This article is licensed under a Creative Commons Attribution-NonCommercial 3.0 Unported Licence.

infrared spectra (FTIR, Nicolet iS5) were measured on a spectrometric analyzer. Solid photoluminescence measurements were obtained on a steady-state/transient fluorescence spectrometer (Edinburgh, FLS920).

Results and discussion

Characterization of 1D $Eu(OH)_3$ nanostructures

Several typical 1D $Eu(OH)_3$ nanocrystals with uniform morphologies were successfully obtained after optimizing the precursor pH and heating temperature of the reaction system. SEM images of the products obtained when the precursors added to the Teflon jar were heated for 25 h are shown in Fig. 1a–e, and the corresponding synthesis conditions and product sizes are listed in Tables 1 and S1 (ESI).† Fig. 1a demonstrates that the short hexagonal prism (SHP) product may be obtained at 120 °C and pH 8.8. When the precursor pH is increased to 9.5 at the same temperature, the hexagonal prisms become more slender and their aspect ratio changes from 1.1 to 2.1 (Fig. 1b). Compared with the SHP product, the long hexagonal prism (LHP) product shows several uneven protrusions approximately 30 nm in diameter at either end, indicating some form of preferential growth direction.

When the hydrothermal temperature and pH are increased to 150 °C and 10.00, respectively, the edges of the original 1D products disappear and the middle portion of the axis develops a groove, similar to coiling rods with hollow ends (CR, Fig. 1c). The average length, diameter, and aspect ratio of the CR product are approximately 258 nm, 48 nm, and 5.3, respectively. The products become short rods (SR) with an aspect ratio of 3.9 at 150 °C and pH 12.00 (Fig. 1d). When the pH is maintained at 12.00 and the temperature of the hydrothermal reaction is raised to 180 °C, long rods (LR, Fig. 1e) with an aspect ratio of 11.8 and low uniformity are obtained. Nanobunches (NB, Fig. 1f) composed of several nanorods attached to each other in parallel with indistinct interfaces are obtained when the hydrothermal reaction is carried out at 150 °C and pH 12.50 for 20 h.

Fig. 2 shows the XRD patterns of the as-obtained six 1D $Eu(OH)_3$ nanostructures. All of the diffraction peaks observed are similar and could be indexed to the pure hexagonal phase of $Eu(OH)_3$ (JCPDS No. 83-2305). The diffraction peaks at 16.1°, 28.1°, and 29.3° correspond to the (100), (110) and (101) planes of $Eu(OH)_3$. Other diffraction peaks could also be attributed to the corresponding crystal planes. Compared with those of other $Eu(OH)_3$ products, the diffraction peaks of NB are relatively weak except for those preferential reflecting the (100), (110), (200) and (300) planes, just like that of $LaVO_4$:Eu^{3+} micro/nanocrystals,[19] which maybe due to its large size and stacking up of several nanorods. Taken together, the XRD results confirm

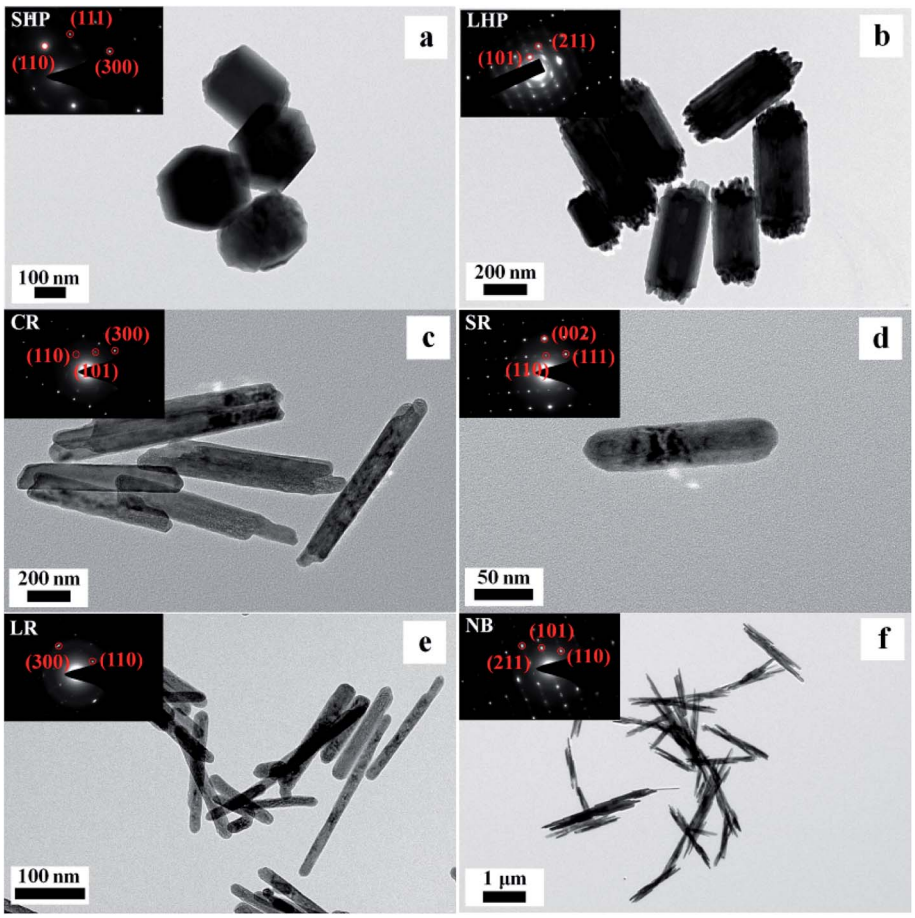

Fig. 3 SEM and SAED (inset) images of the typical $Eu(OH)_3$ nanostructures. (a) SHP. (b) LHP. (c) CR. (d) SR. (e) LR. (f) NB.

 This journal is © The Royal Society of Chemistry 2020

Open Access Article. Published on 10 September 2020. Downloaded on 6/2/2026 2:16:28 AM.
This article is licensed under a Creative Commons Attribution-NonCommercial 3.0 Unported Licence.

that all of the 1D $Eu(OH)_3$ products obtained under hydrothermal conditions have crystalline structures.

TEM images of the six 1D $Eu(OH)_3$ nanostructures obtained *via* hydrothermal synthesis are presented in Fig. 3. In general, all of the products have a solid structure, even texture, and morphologies and sizes consistent with the SEM results (Fig. 3a–f). Small protrusions of different lengths can clearly be seen at both ends of the LHP product. The CR product seems to be formed by the combination of two nanorods that overlap at their junctions, resulting in a smaller outside diameter and larger aspect ratio. And a "gap" appears at both ends of the CR products and the shape of the CR products is similar to hollow.

The inset in Fig. 3 shows the SAED images of the six products; here, the highly single-crystalline nature of the $Eu(OH)_3$ nanostructures, which supports the XRD peaks of the corresponding products shown in Fig. 2, could be clearly observed. The SAED patterns of the six products reveal an ordered lattice, indicating the single-crystal structure of the products. The NB products are composed of several thin single-crystal rods of a relatively large size.

Fig. 4 shows the HRTEM images of the $Eu(OH)_3$ nanostructures. Clear lattice fringes with spacings of 0.317, 0.304, and 0.183 nm respectively corresponding to the (110), (101), and (300) planes of hexagonal-phase $Eu(OH)_3$, consistent with the XRD results, could be seen. These results demonstrate that the morphology, size, and structure of 1D $Eu(OH)_3$ nanostructures can be precisely controlled by changing the reaction conditions of the hydrothermal synthesis process.

The FTIR absorption spectra of the as-prepared $Eu(OH)_3$ nanostructures were recorded over the wavenumber range 400–4000 cm^{-1}, as illustrated in Fig. 5a, to confirm the chemical composition of the products. Interestingly, all of the IR spectra obtained were similar. The sharp peaks at 3609.7 and 699.0 cm^{-1} could be ascribed to the O–H stretching vibrations

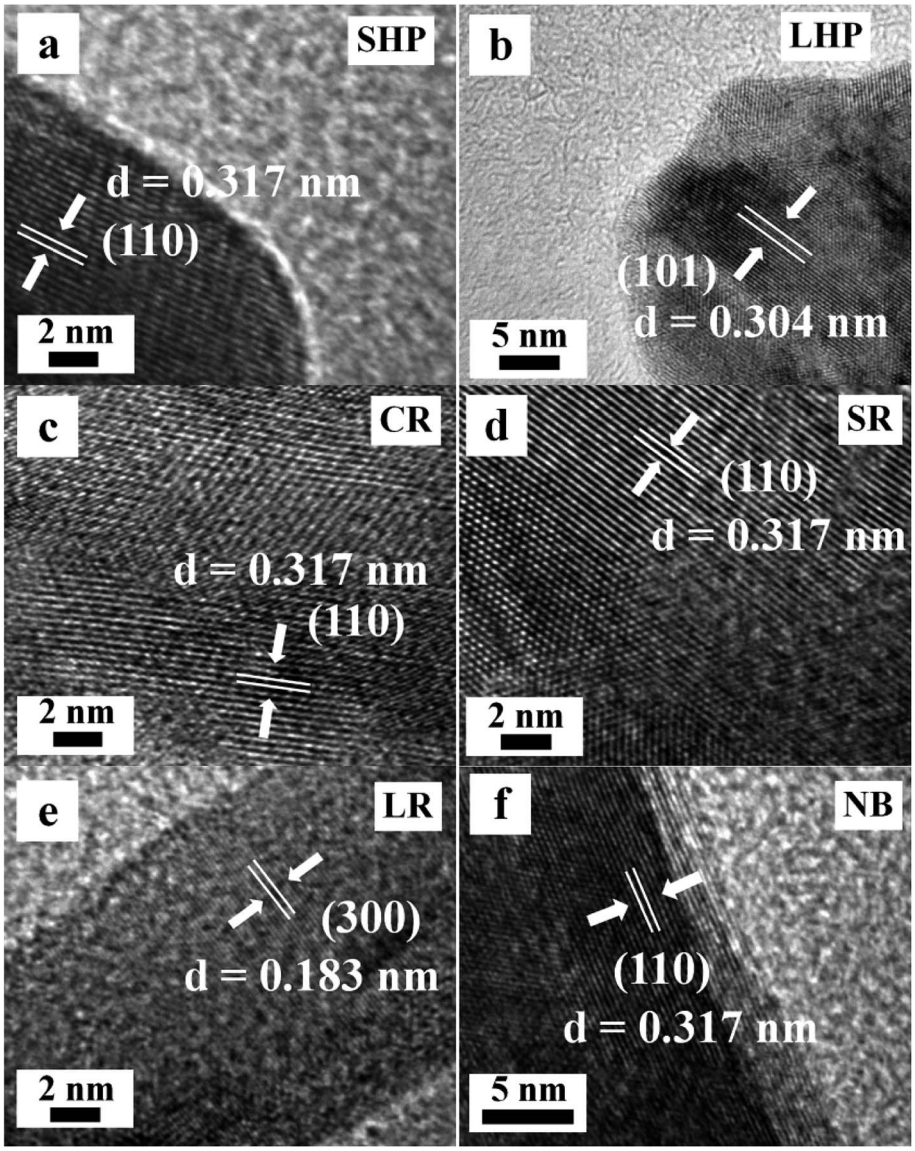

Fig. 4 HRTEM images of the typical $Eu(OH)_3$ nanostructures. (a) SHP. (b) LHP. (c) CR. (d) SR. (e) LR. (f) NB.

Open Access Article. Published on 10 September 2020. Downloaded on 6/2/2026 2:16:28 AM.
This article is licensed under a Creative Commons Attribution-NonCommercial 3.0 Unported Licence.

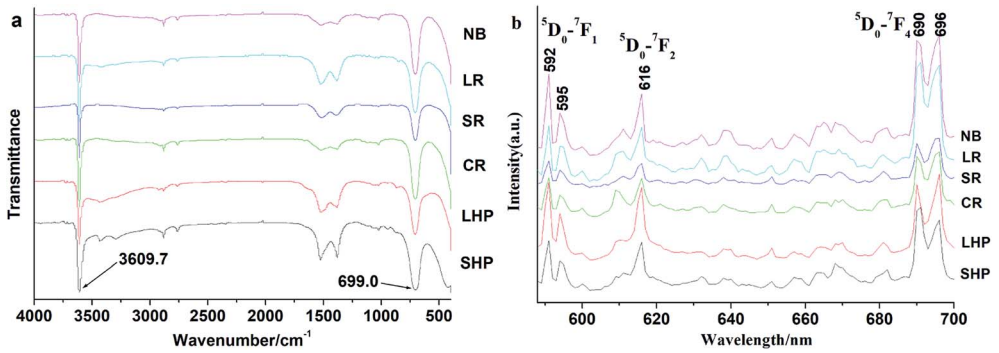

Fig. 5 IR (a) and FL (b) images of the typical $Eu(OH)_3$ nanostructures.

of $Eu(OH)_3$ and Eu–O–H, respectively.[15,16,20] Two weak absorption peaks at 1515.0 and 1390.0 cm^{-1}, which are likely due to the symmetric and asymmetric stretching vibrations of COO^- group, could also be seen; these peaks may have formed from the reaction between absorbed water and CO_2 in air.[21]

Fluorescence properties of 1D $Eu(OH)_3$ nanostructures

The PL spectra of the six $Eu(OH)_3$ products obtained upon excitation at 394 nm and room temperature are shown in Fig. 5b. Six typical emission peaks at 592, 595, 616, 690, and 696 nm could be attributed to the Stark components of the $^5D_0$–^7F_J (J = 1, 2, 4) transition of Eu^{3+}.[14] The peaks at 592 and 616 nm are respectively attributed to the magnetic dipole transitions of $^5D_0$–$^7F_1$ and $^5D_0$–$^7F_2$. These transitions are highly sensitive to the local environment of Eu^{3+}. The intensity of the latter is slight weaker than that of the former, which indicates the high site symmetry of Eu^{3+} in the as-prepared 1D $Eu(OH)_3$ nanostructures.[9,22] If the intensity of the peak at 616 nm is

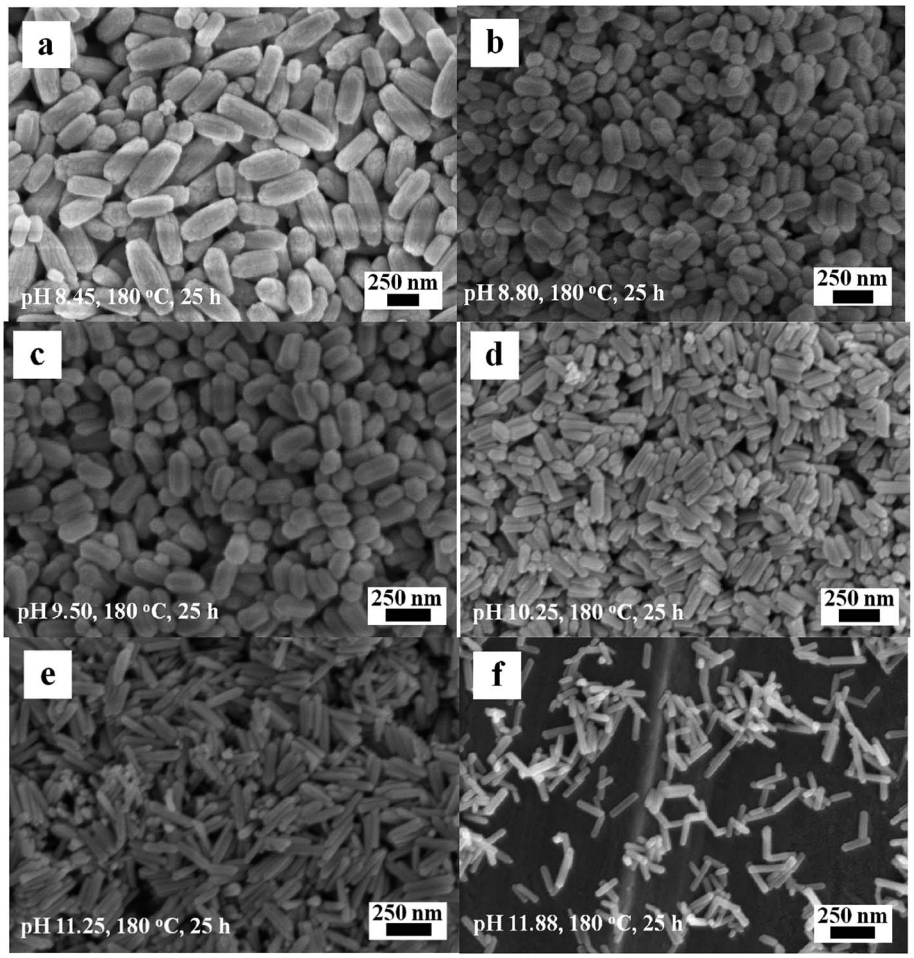

Fig. 6 SEM images of the $Eu(OH)_3$ nanostructures at different pH. (a) 8.45. (b) 8.80. (c) 9.50. (d) 10.25. (e) 11.25. (f) 11.88.

 This journal is © The Royal Society of Chemistry 2020

Open Access Article. Published on 10 September 2020. Downloaded on 6/2/2026 2:16:28 AM.
This article is licensed under a Creative Commons Attribution-NonCommercial 3.0 Unported Licence.

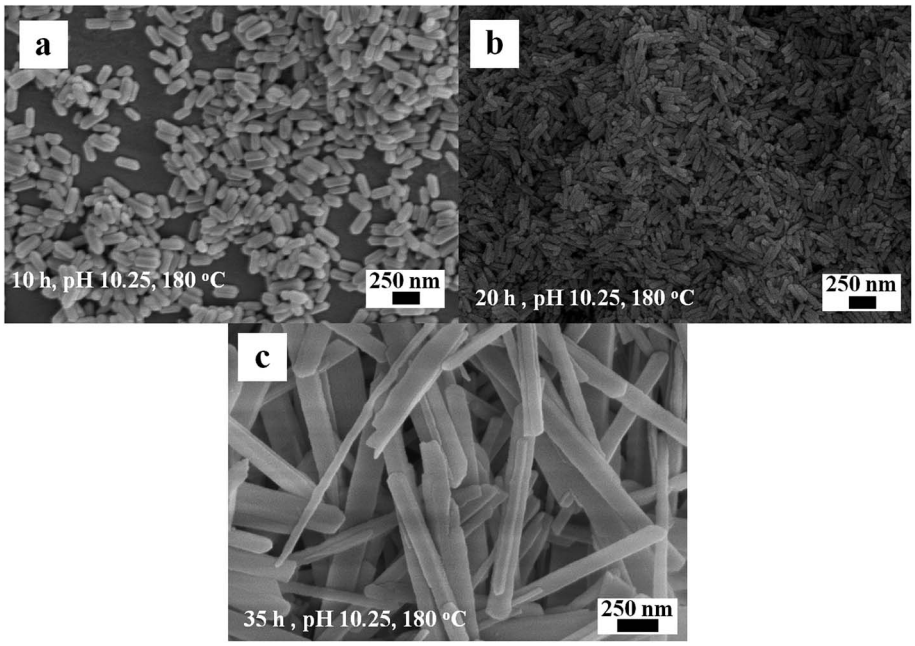

Fig. 7 SEM images of the $Eu(OH)_3$ nanostructures at different reaction time. (a) 10 h. (b) 20 h. (c) 35 h.

significantly higher than that at 592 nm, Eu^{3+} occupies an asymmetric site, which is fairly common in core–shell or doped Eu materials.[23] The emission peaks at 690 nm could respectively be attributed to the $^5D_0$–F_4 transitions of Eu^{3+}. According to the overlapped emission spectra (Fig. S1†) and the λ_{ex}–I curves (Fig. S2†), the solid fluorescence intensities of the 1D $Eu(OH)_3$ products revealed slight changes due to their different microstructure, but the influence is also explainable due to the similar size and 1D shape.

Factors influencing the synthesis of 1D $Eu(OH)_3$ nanostructures

During hydrothermal synthesis, the morphology and size of the $Eu(OH)_3$ products are dramatically affected by the precursor pH, reaction time and temperature. The morphology and size of the products obtained by heating at 180 °C for 25 h under various precursor pH are first explored. At pH 8.45, the products obtained are composed of LHP or elliptical columns of nonuniform length, as shown in Fig. 6a. The prisms become more indistinct and the size uniformity is greatly improved at pH 8.80 (Fig. 6b). The products show as lightly increased aspect ratio but retain their shape as the pH is further increased to 9.50 (Fig. 6c). At pH 10.25 (Fig. 6d) and 11.25 (Fig. 6e), CR-type products of uniform size are obtained; at pH 11.88 (Fig. 6f), the structure of the product changes into LR with uneven lengths. In general, the uniformity of the $Eu(OH)_3$ nanostructures decreases at very high and low pH.

The effect of reaction time (*i.e.*, 10, 20, and 35 h) on the formation of 1D $Eu(OH)_3$ nanostructures was studied under a reaction temperature of 180 °C and pH 10.25. When the reaction time is 10 h, the products show a large size and poor uniformity (Fig. 7a). Little influence on the morphology and size of the $Eu(OH)_3$ products could be observed as the reaction time is increased from 10 h to 20 h at pH 10.25 (Fig. 7b). However, when the reaction time is 35 h, the products reveal a larger size and more uneven morphology compared with those obtained at 10 h (Fig. 7c). These results indicate that crystal growth process may play some supporting role in the final morphology of the products late in the hydrothermal reaction.[24]

The synergistic effects of reaction time and precursor pH on the morphology and size of the products were investigated by cross experiments at a constant temperature (180 °C) to obtain the optimal conditions for the formation of the 1D $Eu(OH)_3$. Fig. 8a–f demonstrate that the precursor pH results in obvious changes in the morphology of $Eu(OH)_3$ nanostructures when all other conditions are held constant. However, comparing the images of Fig. 8c and f, their morphologies were some different, some thin rods coexisted with chick rods by increasing time from 10 to 20 h at same temperature. It indicate that pH is still the main factor affecting the morphology of 1D $Eu(OH)_3$ nanostructures, and the reaction time also partly affects the size and morphological uniformity of the products when the pH value is determined.

Fig. 9 illustrates the SEM images of the $Eu(OH)_3$ products obtained at 150 °C and 180 °C during hydrothermal treatment at 25 h and pH 9.5. Compared with the products prepared at 120 °C (Fig. 1b), smaller irregular hexagonal prisms are obtained when the temperature is 150 °C; moreover, the edges of the latter are more vague and protrusions are not observed at either end of the nanoprisms (Fig. 9a). At 180 °C, the definition and evenness of the edges of the products decrease and the two ends of the products become sharper and rounder (Fig. 9b). The mean size of the products increases slightly as the temperature increases, similar to the results of hydroxyapatite nanocrystals synthesized *via* the hydrothermal method.[24] Taking the results together, the nanostructures of $Eu(OH)_3$ could be well regulated

Open Access Article. Published on 10 September 2020. Downloaded on 6/2/2026 2:16:28 AM.
This article is licensed under a Creative Commons Attribution-NonCommercial 3.0 Unported Licence.

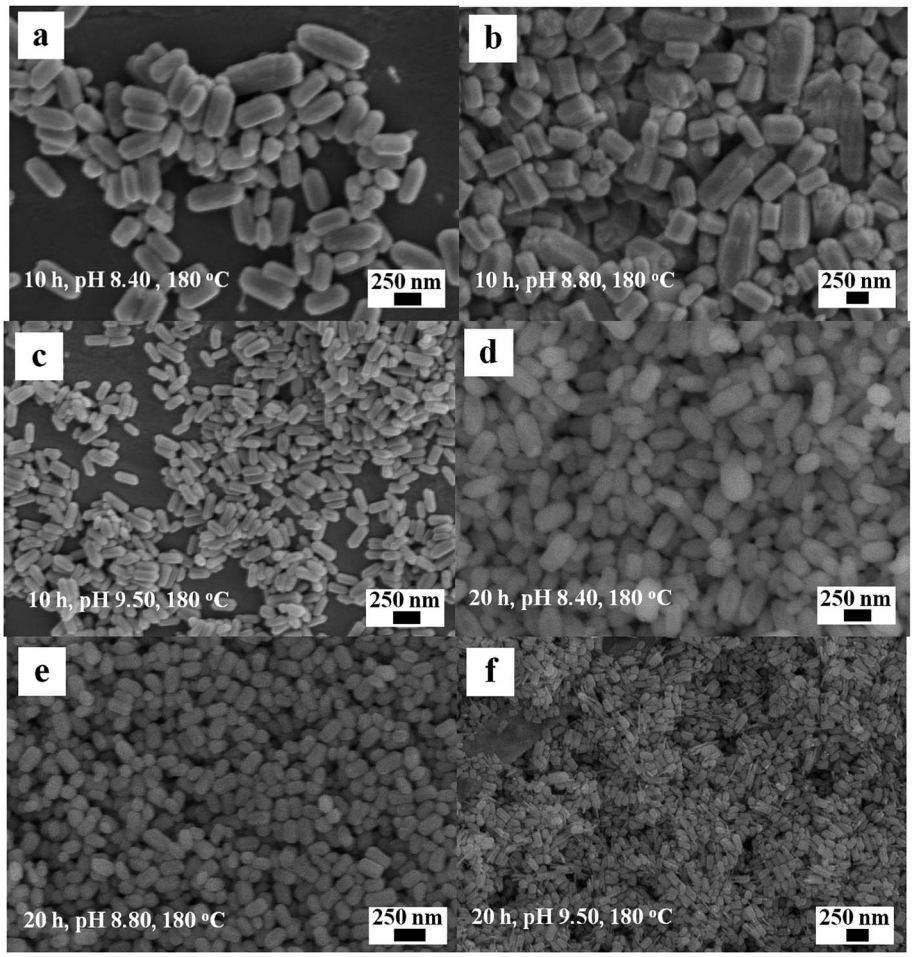

Fig. 8 SEM images of the $Eu(OH)_3$ nanostructures at different reaction time and pH. (a) 10 h, pH 8.40. (b) 10 h, pH 8.80. (c) 10 h, pH 9.50. (d) 20 h, pH 8.40. (e) 20 h, pH 8.80. (f) 20 h, pH 9.50.

by precisely adjusting the precursor pH, reaction time and temperature, resulting in the formation of 1D nanomaterials with diverse morphologies and uniform sizes.

Growth mechanism of 1D $Eu(OH)_3$ nanostructures

Based on the above experimental results under different synthesis conditions, the formation of 1D $Eu(OH)_3$ nanostructures involved two growth processes of nucleation and aggregation growth, which can be proposed as follows. Firstly, a large number of small nuclei composed of 1D hexagonal crystals rose in its anisotropic growth nature[25] are rapidly formed in the supersaturated precursor solution on account of the reaction between Eu^{3+} and OH^- derived from the precursor gel. Secondly, the hexagonal crystal nuclei will continue to grow under the synergistic influence of precursor pH, temperature and reaction time on the hydrothermal reaction system.[10] During the latter process (*i.e.* aggregation growth), the precursor pH strongly affects the formation of these nanostructures because OH^- not only is a source to form $Eu(OH)_3$, but also acts as a capping agent for changing the polar

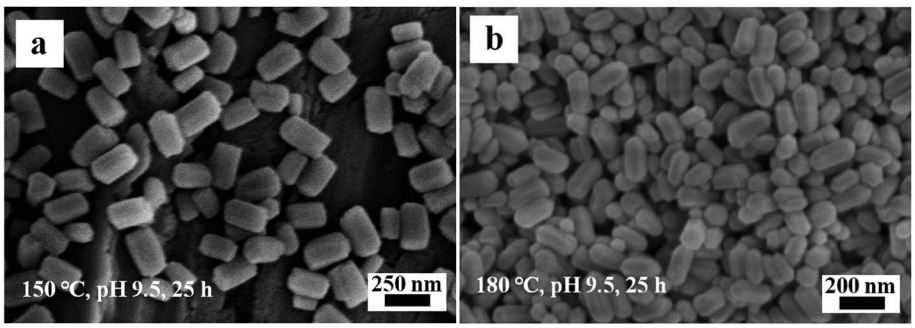

Fig. 9 SEM images of the $Eu(OH)_3$ nanostructures at different temperature. (a) 150 °C. (b) 180 °C.

 This journal is © The Royal Society of Chemistry 2020

Open Access Article. Published on 10 September 2020. Downloaded on 6/2/2026 2:16:28 AM.
This article is licensed under a Creative Commons Attribution-NonCommercial 3.0 Unported Licence.

surface energy of crystals, especially at excessively high or low OH^- concentrations.[26] The preferential adsorption crystal planes of OH^- ions are variable with increasing the concentration of OH^-, which resulting in different growth rates in different planes.[27] When the pH kept constant, other factors will produce a marked effect. The aggregation growth of nanocrystals is further affected by not only reaction time but also temperature,[28] which can affects the size and uniformity of $Eu(OH)_3$ morphology.[16] It is well known that the influence factors of the formation of nanostructures are many and complicated in the hydrothermal reaction system.[29,30] Besides the above three factors, the reactant concentration, solution volume, system pressure, *etc.* may also affect the geometric characteristics and microstructures of the nanomaterials obtained from the hydrothermal process. So the exact growth mechanism for the formation of these 1D $Eu(OH)_3$ nanostructures should be further confirmed from multiple aspects.

Conclusions

In summary, six uniform and single-crystalline 1D $Eu(OH)_3$ nanostructures with different morphologies were successfully fabricated *via* the hydrothermal method. All as-prepared 1D $Eu(OH)_3$ nanostructures presented good fluorescence properties, and a possible growth mechanism was proposed. Several factors, such as the precursor pH, reaction time and temperature, could affect the formation of the $Eu(OH)_3$ crystals. In particular, the precursor pH strongly influenced the growth of the $Eu(OH)_3$ products.

Conflicts of interest

There are no conflicts to declare.

Acknowledgements

This work was financially supported by the Natural Science Foundation of Anhui Province of China (2008085ME124), the Key Research and Development Projects in Anhui Province (202004d07020005), the Research Activity Funding Project for Academic and Technical Leaders and Reserve Candidates in Anhui Province of China (2019H227), the Anhui Province Academic Support Project for Top Talents of Disciplines (majors) in Colleges and Universities (gxbjZD2020070), the Anhui Province Laboratory of Molecule-Based Materials (fzj19016), and the College Students' Innovation and Entrepreneurship Program of Anhui Province of China (201810368134, 201910368039). We also thank Anhui Provincial Engineering Research Center for Polysaccharide Drugs, Provincial Engineering Laboratory for Screening and Re-evaluation of Active Compounds of Herbal Medicines in Southern Anhui, and B. S. Peiqi Shi for help this work.

References

1 G. Chen, H. Wan, W. Ma, N. Zhang, Y. J. Cao, X. H. Liu, J. Wang and R. Z. Ma, Layered metal hydroxides and their derivatives: controllable synthesis, chemical exfoliation, and electrocatalytic applications, *Adv. Energy Mater.*, 2019, **10**, 1902535.

2 H. L. Liu, F. Nosheena and X. Wang, Noble metal alloy complex nanostructures: Controllable synthesis and their electrochemical property, *Chem. Soc. Rev.*, 2015, **44**(10), 3056–3078.

3 X. Z. Li, K. L. Wu, Y. Ye and X. W. Wei, Gas-assisted growth of boron-doped nickel nanotube arrays: Rapid synthesis, growth mechanisms, tunable magnetic properties, and super-efficient reduction of 4-nitrophenol, *Nanoscale*, 2013, **5**, 3648–3653.

4 Z. L. Wang, ZnO nanowire and nanobelt platform for nanotechnology, *Mater. Sci. Eng., R*, 2009, **64**(3–4), 33–71.

5 X. Z. Li, P. J. Hu, Y. Y. Cao, G. X. Zhu and X. P. Shen, Composition-tunable $Ni_{1-x}Co_x$ nanotubes: Template synthesis, magnetic properties, and catalytic activities for the reduction of 4-nitrophenol, *Mater. Lett.*, 2018, **228**, 387–390.

6 A. W. Xu, Y. Gao and H. Q. Liu, The preparation, characterization, and their photocatalytic activities of rare-earth-doped TiO_2 nanoparticles, *J. Catal.*, 2002, **207**, 151–157.

7 D. Lee, J. Seo, L. d. l. S. Valladares, O. A. Quispe and C. H. W. Barnes, Magnetic and structural properties of yellow europium oxide compound and $Eu(OH)_3$, *J. Solid State Chem.*, 2015, **228**, 141–145.

8 L. Zhang, W. L. Hu, Y. D. Wu, P. F. Wei, L. Dong, Z. Y. Hao, S. Fan, Y. H. Song, Y. Lu, C. Z. Liang and L. P. Wen, Microwave-assisted facile synthesis of $Eu(OH)_3$ nanoclusters with pro-proliferative activity mediated by miR-199a-3p, *ACS Appl. Mater. Interfaces*, 2018, **10**, 31044–31053.

9 A. A. Ansari, T. N. Hasan, N. A. Syed, J. P. Labis, A. K. Parchur, G. Shafi and A. A. Alshatwi, In-vitro cyto-toxicity, geno-toxicity, and bio-imaging evaluation of one-pot synthesized luminescent functionalized mesoporous SiO_2@$Eu(OH)_3$ core-shell microspheres, *Nanomed. Nanotechnol.*, 2013, **9**, 1328–1335.

10 D. S. Zhang, T. T. Yan, L. Y. Shi, H. R. Li and J. F. Chiang, Template-free synthesis, characterization, growth mechanism and photoluminescence property of $Eu(OH)_3$ and Eu_2O_3 nanospindles, *J. Alloys Compd.*, 2010, **506**, 446–455.

11 N. Du, H. Zhang, B. D. Chen, J. B. Wu, D. S. Li and D. R. Yang, Low temperature chemical reaction synthesis of single-crystalline Eu(OH)3nanorods and their thermal conversion to Eu_2O_3 nanorods, *Nanotechnology*, 2007, **18**, 065605.

12 K. Kattel, J. Y. Park, W. L. Xu, B. A. Bony, W. C. Heo, T. Tegafaw, C. R. Kim, M. W. Ahmad, S. Jin, J. S. Baeck, Y. M. Chang, T. J. Kim, J. E. Bae, K. S. Chae, J. Y. Jeong and G. H. Lee, Surface coated $Eu(OH)_3$nanorods: A facile synthesis, characterization, MR relaxivities and *in vitro* cytotoxicity, *J. Nanosci. Nanotechnol.*, 2013, **13**(11), 7214–7219.

Open Access Article. Published on 10 September 2020. Downloaded on 6/2/2026 2:16:28 AM. This article is licensed under a Creative Commons Attribution-NonCommercial 3.0 Unported Licence.

13 X. F. Yang, G. L. Ning and Y. Lin, Preparation of $Eu(OH)_3$ and Eu_2O_3 nanorods through a simple method, *Chem. Lett.*, 2007, **36**(3), 468–469.

14 Q. G. Zeng, Z. J. Ding, Z. M. Zhang and Y. Q. Sheng, Photoluminescence and Raman spectroscopy studies of $Eu(OH)_3$ rods at high pressures, *J. Phys. Chem. C*, 2010, **114**, 4895–4900.

15 J. G. Kang, Y. Jung, B. K. Min and Y. Sohn, Full characterization of $Eu(OH)_3$ and Eu_2O_3 nanorods, *Appl. Surf. Sci.*, 2014, **314**, 158–165.

16 H. Wu, Y. J. Zhang, M. Z. Zhou, C. P. Yao and X. J. Ge, Growth of $Eu(OH)_3$ large single crystals by solid KOH assisted hydrothermal method and luminescent and magnetic properties, *Cryst. Res. Technol.*, 2016, **51**(9), 508–512.

17 X. Z. Li, K. L. Wu, Y. Ye and X. W. Wei, Controllable synthesis of Ni nanotube arrays and their structure-dependent catalytic activity toward dye degradation, *CrystEngComm*, 2014, **16**, 4406–4413.

18 X. Z. Li, K. L. Wu, C. Dong, S. H. Xia, Y. Ye and X. W. Wei, Size-controlled synthesis of Ag_3PO_4 nanorods and their high-performance photocatalysis for dye degradation under visible-light irradiation, *Mater. Lett.*, 2014, **130**, 97–100.

19 Y. Q. Zhu, Y. H. Ni and E. H. Sheng, Fluorescent $LaVO_4$:Eu^{3+} micro/nanocrystals: pH-tuned shape and phase evolution and investigation of the mechanism of detection of Fe^{3+} ions, *Dalton Trans.*, 2016, **45**, 8994–9000.

20 K. L. Wong, G. L. Law, M. B. Murphy, P. A. Tanner, W. T. Wong, P. K. Lam and M. H. Lam, Functionalized europium nanorods for *in vitro* imaging, *Inorg. Chem.*, 2008, **47**, 5190–5196.

21 Y. Li, C. P. Ooi and P. H. N. Cheang, Synthesis and characterization of neodymium (III) and gadolinium (III)-substituted hydroxyapatite as biomaterials, *Int. J. Appl. Ceram. Technol.*, 2009, **6**(4), 501–512.

22 S. Dasgupta, R. K. Mukherjee, S. Mroczkowski and D. Ghosh, Magnetic susceptibilities of $Eu(OH)_3$: effects of crystal-field and anisotropic exchange coupling, *J. Phys. C: Solid State Phys.*, 1988, **21**, 3339.

23 A. K. Parchur and R. S. Ningthoujam, Preparation and structure refinement of Eu^{3+} doped $CaMoO_4$ nanoparticles, *Dalton Trans.*, 2011, **40**, 7590–7594.

24 Y. Zhu, L. L. Xu, C. H. Liu, C. N. Zhang and N. Wu, Nucleation and growth of hydroxyapatite nanocrystals by hydrothermal method, *AIP Adv.*, 2018, **8**, 085221.

25 B. Q. Cao and W. P. Cai, From ZnO nanorods to nanoplates: Chemical bath deposition growth and surface-related emissions, *J. Phys. Chem. C*, 2008, **112**(3), 680–685.

26 Y. Zhang, J. Q. Xu, Q. Xiang, H. Li, Q. Y. Pan and P. C. Xu, Brush-like hierarchical ZnO nanostructures: synthesis, photoluminescence and gas sensor properties, *J. Phys. Chem. C*, 2009, **113**(9), 3430–3435.

27 L. Zhu, J. Meng and X. Q. Cao, Facile synthesis and photoluminescence of europium ion doped LaF_3 nanodisks, *Eur. J. Inorg. Chem.*, 2007, **24**, 3863–3867.

28 H. Zhang, D. H. Ha, R. Hovden, L. F. Kourkoutis and R. D. Robinson, Controlled synthesis of uniform cobalt phosphide hyperbranched nanocrystals using tri-n-octylphosphine oxide as a phosphorus source, *Nano Lett.*, 2011, **11**(1), 188–1970.

29 L. Zhen, W. S. Wang, C. Y. Xu, W. Z. Shao and L. C. Qin, A facile hydrothermal route to the large-scale synthesis of $CoWO_4$ nanorods, *Mater. Lett.*, 2008, **62**(10–11), 1740–1742.

30 S. K. Hussain, G. Nagaraju, E. Pavitra, G. S. R. Raju and J. S. Yu, $La(OH)_3$:Eu^{3+} and La_2O_3: Eu^{3+} nanorod bundles: growth mechanism and luminescence properties, *CrystEngComm*, 2015, **17**, 9431–9442.

 This journal is © The Royal Society of Chemistry 2020